Image Cover Sheet

CLASSIFICATION	SYSTEM NUMBER
UNCLASSIFIED	507218

TITLE

DEVELOPMENT OF AN OPTIMUM CONSUMABLE ALLOY FOR LOW HEAT INPUT WELDING OF NICKEL ALUMINUM BRONZES

System Number:

Patron Number:

Requester:

Notes: Paper #15 contained in Parent Sysnum #507203

DSIS Use only:

Deliver to: DK

#507218 (15)

Development of an Optimum Consumable Alloy for Low Heat Input Welding of Nickel Aluminum Bronzes

by

C.V. Hyatt[1], J.C. Bennett[2], G. Pelletier[1], B. Armstrong[1], K. KarisAllen[3], J. Hewitt[4], T. Betancourt[6] J. Gianetto[5] and M. Sahoo[5].

ABSTRACT

Nickel aluminum bronzes are used in ship and submarine sea water handling, propulsion and combat systems equipment, as well as in a range of commercial high performance components. Usually, when these alloys fail, they fail by a surface sensitive mechanism such as wear, corrosion, dealloying, cavitation-erosion or corrosion fatigue. To determine if these surface properties could be improved with laser cladding, a laser cladding method was developed and the processing-structure-property relationships were studied. Microstructures and properties were found to be highly dependent on heat input. To reduce this sensitivity to heat input and further improve properties, work to develop an optimum consumable alloy was undertaken. The effects of additions of chromium, zirconium, and titanium were investigated along with the effects of composition variation within the range allowed by various standards. Work so far reveals three possible alloying approaches. Using these alloying approaches, reductions in the sensitivity of microstructures to heat input and property improvements are possible.

1. Defence Research Establishment Atlantic, Dartmouth, Nova Scotia, Canada
2. Acadia University, Wolfville, Nova Scotia, Canada
3. FACTS Engineering, Halifax, Nova Scotia, Canada
4. The Laser Institute, Edmonton, Alberta, Canada
5. Materials Technology Laboratory, Ottawa, Canada
6. Nova Scotia Research Foundation (now retired)

1.0 INTRODUCTION

Nickel aluminum bronzes are, and will remain for the foreseeable future, the most important alloy used in ship and submarine propulsion and sea water handling systems[1,2]. They are also extensively used in combat systems equipment. In all marine applications the performance of these alloys is limited by surface sensitive properties—corrosion-fatigue for propellers, crevice corrosion for valves, cavitation-erosion for pumps and wear for bearings[3-8]. It is also significant that many high value-added components made of nickel aluminum bronzes cannot be reclaimed by current welding methods because of some localized corrosion problems as well as distortion problems[5-8]. These problems are believed, at least in part, to be caused by poor understanding of effects of heat input and composition (especially residual elements) on the microstructure and properties of nickel aluminum bronze weldments. Clearly large improvements in performance are possible by improving the surface properties of nickel aluminum bronzes. Recent analysis' of the through life costs of warships show that extending the life of nickel aluminum bronze components would also have cost benefits as well. Low heat input welding and weld cladding methods such as laser welding are promising means to improve the surface properties of nickel aluminum bronzes and to make repairs which we cannot make now[9-25].

To overcome the problems just mentioned, DREA has been investigating the surface engineering and clad welding of nickel aluminum bronzes. The goals of this project are to develop means to improve equipment performance and reduce operation and maintenance costs. This can be done by engineering the surfaces of components to make them last longer and by making possible repairs which are impossible with current technology. Goals of the work include:

1. Developing low heat input laser welding methods for cladding complex shapes with minimal distortion, as well as higher heat input processes;

2. Evaluating the properties and in-service performance of laser clad materials and components, which involves the development of new experimental techniques;

3. Developing optimum alloys, with high hardness, ductility and resistance to all forms of corrosion when deposited with a range of heat inputs; and

4. Seeing the procedures and materials put into practice, first for repair and later for the treatment of new components.

Previously, we reported that a low heat input laser cladding method had been developed and showed that complex parts of ships and submarines could be clad for a reasonable cost [21,28,29]. We also reported on the structure of deposits and on the effect of heat input in laser cladding[21,22,30].

In the heat input study, nickel aluminum bronze castings were clad with a consumable of composition Cu-9.0 Al-4.6 Ni-3.9-Fe-1.2 Mn and a range of heat inputs from 42.5 to 595

J/mm. At the lowest heat input, the deposit microstructure was almost entirely martensitic. Increases in heat input caused the amount of α to increase. Depending upon heat input, the α was present as grain boundary allotriomorphs, secondary Widmanstätten α sideplates and intragranular Widmanstätten α precipitates. The reheated zones were of lower hardness, and at all heat inputs consisted of a mixture of grain boundary allotriomorphs and Widmanstätten α and martensite. Laser cladding improved the corrosion and cavitation erosion resistance of the surfaces but reduced their ductility. Properties of the clad surfaces depended on heat input [30]. Other work showed that deposit composition also effects microstructure [31].

Laser cladding would be more useful for nickel aluminum bronzes if the microstructures and properties were less sensitive to heat input, if further property improvements could be made and if reductions in ductility could be eliminated through the development of a nickel aluminum bronze consumable alloy, optimum for the low heat input welding. Such an alloy should be insensitive to heat input (hopefully though not likely, even in conventional welding), have high hardness and better ductility, high resistance to corrosion, de-alloying, wear, cavitation and erosion corrosion, pitting and corrosion fatigue and have a corrosion potential similar to that of nickel aluminum bronze

There is good reason to believe this goal is achievable. First, as mentioned above, microstructural response to heat input and probably properties, do depend on heat input. Second, data on solid state quenching shows that nickel and iron content and the Ni/Fe ratio as well as Al content affects hardenability [32]. Third, a variety of additions including Zr, Ti, and Cr give hardening in other copper alloys including bronzes. These elements are particularly interesting, because some early patents suggest these elements inhibit both dealloying and stress corrosion in cast and wrought aluminum bronzes[2 and references therein]. Finally, data on ternary intermetallics suggests a number of potentially useful strengthening precipitates might form from the addition of these elements [33, 34].

To identify an optimum alloy composition, 28 experimental alloys, laser surface melted with eight different heat inputs were examined. So far microstructures, microhardnesses, cavitation erosion behaviors, corrosion potentials and temper resistance by resistivity have been investigated. These are the topics of this paper. Wear, erosion-corrosion, long term immersion (including crevice corrosion), potentiodynamic corrosion, differential thermal analysis and corrosion-fatigue studies are planned.

2.0 MATERIALS AND METHODS

The compositions of the experimental alloy castings used in this work are shown in Table 1. To simply investigate heat input effects, surface melting (autogenous welding) was performed using the conditions listed in Table 2. Optical metallography and some transmission electron microscopy was also carried out using the preparation techniques summarized in Refs. 30,35,36. We describe the resolidified laser melt as the remelted material (analogous to the as-deposited in a clad deposit) and the heat affected zone in the remelted material produced by the next pass as the reheated zone (analogous to the reheated zone in a clad deposit)

⊕ **Table 1. Nickel Aluminum Bronze Alloy Compositions**

Series	Melt #	Sample	Cu	Ni	Fe	Mn	Al	Cr	Ti	Zr	Ni/Fe
C	103.95-2	1	76.45	5.06	6.20	0.35	9.70		2.24		0.82
B	125.95-3	2	79.60	3.80	5.50	1.00	10.10				0.69
B	128.95-1	3	80.10	5.00	4.70	1.10	9.10				1.06
B	125.95-1	4	81.20	3.80	3.90	1.00	10.10				0.97
B	128.95-2	5	78.60	6.50	4.60	1.10	9.20				1.41
B	133.95-1	6	78.00	4.70	3.80	1.30	12.20				1.24
B	132.95-3	7	77.95	4.00	5.80	0.95	11.30				0.69
A	124.95-1	8	80.20	4.60	4.80	1.10	9.30				0.96
A	124.95-3	9	77.30	4.60	4.60	1.00	12.50				1.00
C	103.95-3	10	75.44	4.95	6.10	0.36	9.60		3.55		0.81
A	124.95-2	11	78.80	4.70	4.70	1.10	10.70				1.00
B	132.95-1	12	79.30	4.10	4.30	1.00	11.30				0.95
B	133.95-2	13	76.40	5.90	4.20	1.30	12.20				1.40
C	103.95-1	14	77.20	5.05	6.30	0.31	10.00		1.08		0.80
B	133.95-3	15	74.00	6.10	6.50	1.20	12.20				0.94
B	132.95-2	16	78.60	4.10	5.00	1.00	11.30				0.82
B	128.95-3	17	77.60	6.50	5.70	1.00	9.20				1.14
C	114.95-1	18	77.83	4.95	6.02	0.83	9.40			0.97	0.82
A	136.95-1	19	79.30	4.60	6.20	1.10	8.80				0.74
C	137.95-2	20	77.23	5.16	5.60	1.10	9.76	1.15			0.92
C	137.95-1	21	78.71	5.19	4.78	1.10	9.61	0.61			1.09
A	136.95-3	22	78.40	4.60	6.20	1.10	9.70				0.74
D	140.95-2	23	78.95	4.70	5.00	1.00	8.90	0.60	0.44	0.41	0.94
	140.95-3	24	80.60	3.70	4.40	0.91	7.80	1.12	0.79	0.68	0.84
C	137.95-3	25	76.14	5.10	6.30	1.10	9.64	1.72			0.81
A	136.95-2	26	78.90	4.60	6.10	1.10	9.30				0.75
D	140.95-1	27	78.63	4.90	5.30	1.10	9.30	0.31	0.23	0.23	0.92

Table 2. Laser Surface Melting conditions

Condition (#)	Laser	Heat Input (J/cm)	Ave. Power (w)	Speed		Melt Pool	Defocus
				(cm/s)	(ipm)	Width (um)	(mm)
1	Mits	25	800	32.0	756	275	0.00
2	Mits	100	800	8.0	189	360	0.00
3	CE5000	650	5000	7.7	182	1100	10.80
4	CE5000	800	5000	6.3	148	1100	10.80
5	CE5000	1000	5000	5.0	118	1200	10.80
6	CE5000	1500	5000	3.3	79	1500	10.80
7	CE5000	3000	5000	1.7	39	1800	11.30
8	CE5000	3000	5000	1.7	39	1700	10.80
9	CE5000	650	5000	7.7	182	1100	10.80
10	CE5000	3000	5000	1.7	39	1800	11.30

Corrosion potentials (E_{corr}) were determined by the ASTM G5 method [37]. Briefly, after wires were attached to the surface melted specimens, the specimens were mounted in epoxy so that only the laser surface melted face was measured. Except in a few cases where

deliberate exceptions were made, the surface melted face was ground to remove the oxide layer prior to testing. The corrosion potentials were measured with respect to a standard calomel electrode in de-aerated sea water at 25 °C. Measurements were made after 1 hour of immersion.

Cavitation erosion measurements were made according to ASTM standard G-32 [38]. The experimental test apparatus consisted of a Branson Model No. 108 connected to a 184V power supply/function generator. A 1:1 booster was attached between the titanium horn and the converter. The specimens were attached at the lower extremity of the horn which was submerged in sea water during testing. Sea water temperature was maintained at $25\ ^0C \pm 2\ ^0C$ during testing. As well, a peak to peak amplitude of 0.05 mm was maintained throughout the test and the operating frequency of the horn was maintained at 20 kHz. For each run, a two liter beaker was filled with naturally occurring sea water and placed in the water bath. A 316 stainless steel specimen was run in the sea water for 30 minutes to stabilize the gas content. The specimen was then screwed into the horn tip and pretorqued to 120 in-lbf with a torque wrench. The test apparatus holder slid vertically on a rod at the back of the cabinet. The holder was positioned so that the face of the test specimen was immersed approximately 10 mm in the test liquid. The power was activated and the voltage adjusted to between 152 Vdc and 154 Vdc.

Test duration was approximately 16-20 hours. For the first half of the test, the specimen was removed from the horn every hour, washed with acetone, blown dry and weighed using an analytical scale. For the second half of the test, this procedure was repeated every two hours. When the test was completed, the weight of the specimen was recorded and the specimen stored in a desiccator.

Temper resistance of the different alloys was assessed by electrical resistance measurements. Samples approximately 1.00 mm thick, 3.00 mm wide and 40.00 mm in length were heat treated at 1000°C for one hour, quenched in an iced brine solution, and then tempered at temperatures from 400°C to 900°C for various times.

3.0 RESULTS

3.1. Metallography and Microhardness

Work on the metallography of the alloy set is in progress. So far optical metallography has been completed on all specimens for laser surface melting conditions 10, 65 and 300 J/mm. This work will be reported in detail in a DREA report [39]. A report on the base casting structures is also to be available shortly.

Briefly, work on the laser melted experimental alloys showed remelted and reheated zone microstructures were affected strongly by composition and heat input. Hardness as a function of the alloy numbers listed in Table 1, for several different heat inputs is shown in Fig. 1. Replotting this as a function of aluminum content (Ni/Fe ratios are shown beside each point), shows that higher aluminum favors a both higher remelted hardness and increased resistance

to softening of the reheated zone. As well Ni/Fe ratio seems to affect hardness. This requires further investigation, though it appears that above 10 % Al, Ni/Fe greater than 1 favors higher hardness while below 10% Al the effect is reversed. .

The non-standard additions provided some hoped for increases in hardness. First, in the remelted material, both Ti and Cr increase remelted hardness relative to an otherwise similar alloy without these additions. Of significance relative to the design of an alloy which will retain high hardness over a range of heat inputs is the observation that for Ti additions a peak in the hardening effect occurred at 65 J/mm while for Cr additions hardness as a function of heat input was still increasing at 300 J/mm. It is also clear from the data that Cr, Zr, Ti all reduce sensitivity of the reheated zone to tempering, and give harder reheated zones than for otherwise equivalent alloys which do not contain these additions. The results show Cr and Ti additions are particularly effective additions for improving resistance to tempering.

The reason for the observed reversal in the effect of Ni/Fe ratio as aluminum content increases is unclear. Possibly at low aluminum, the Ni/Fe ratio may be more important in determining hardenability and whether or not lower hardness bainites or α phases form, while at high aluminum only martensitic microstructures form so the effect of Ni/Fe on martensite structure, order, and precipitate type and coherency probably becomes more important. Alternatively, in the low aluminum case, the Ni/Fe ratio may affect precipitate type, size and density. Electron microscopy studies now in progress may clarify this issue.

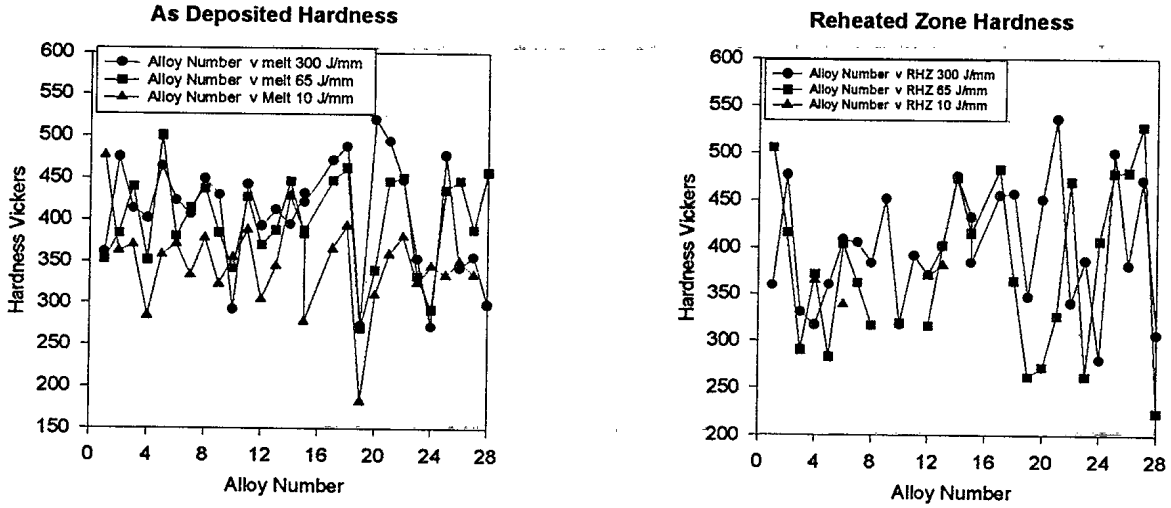

a. b.

Figure 1. Hardness of as deposited (a) and reheated zones (b) as a function of heat input.

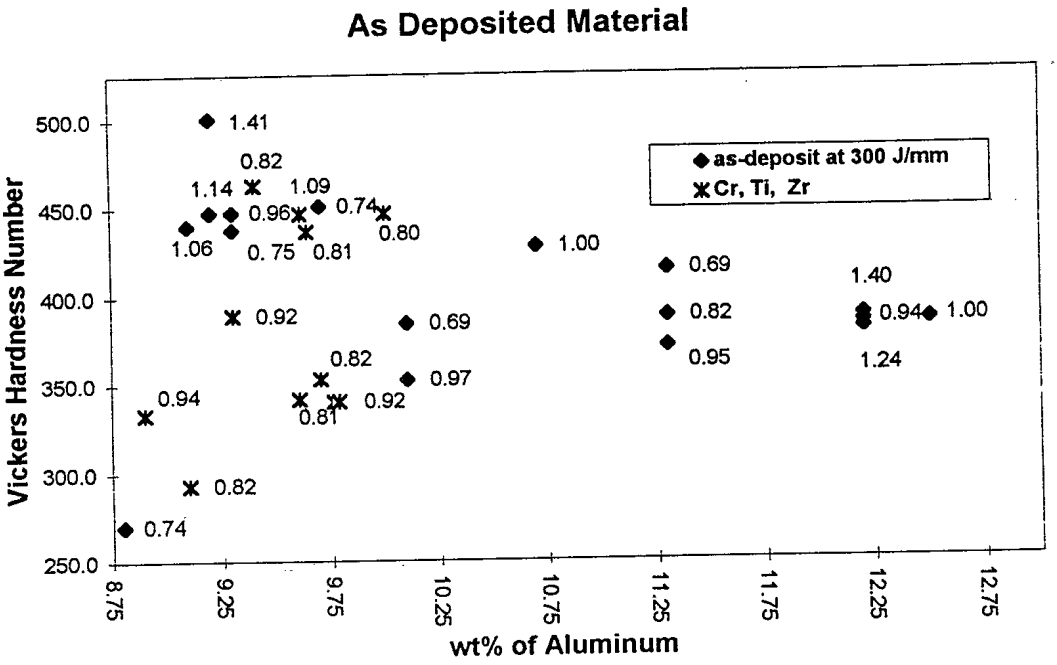

a.

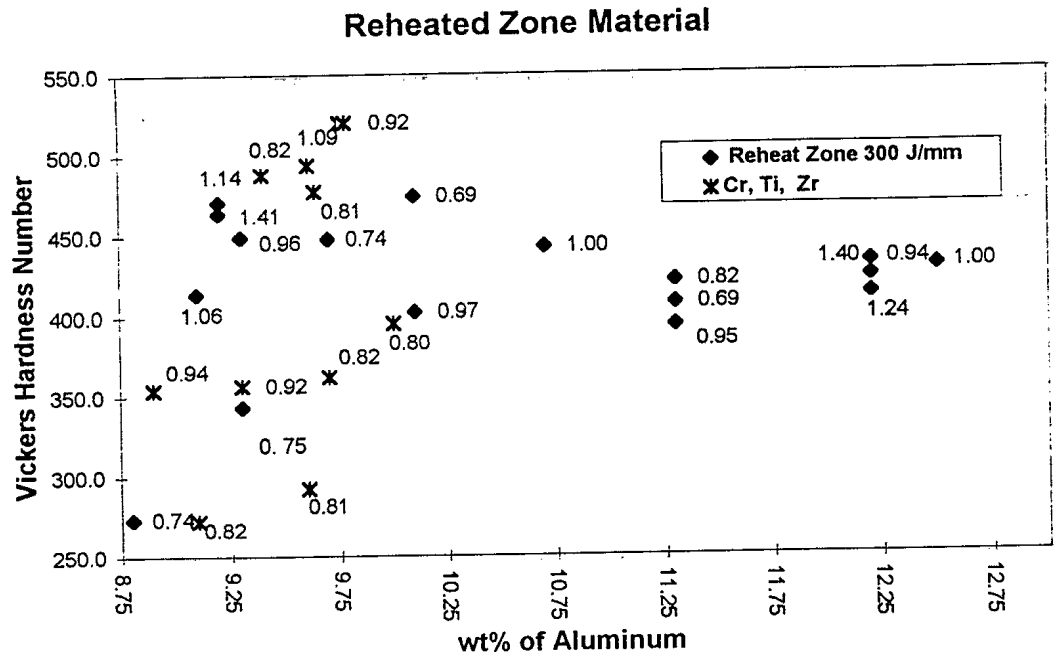

b.

Figure 2. Remelted (a) and reheated (b) zone hardness as a function of aluminum content

We plan to discuss the details of the effects of heat input and composition on the microstructure of these alloys in several future papers. Work so far has revealed some

interesting trends. First, as the aluminum content is increased, the volume fraction of α becomes lower. Above 11% Al, no α is present in the deposit, even at relatively high heat inputs of 300 J/mm. For Al contents of less than about 9 %, little high temperature β phase forms so there are few β transformation products, only a dendritic solidification structure. Examples of these two extremes are shown in Figs. 3 and 4. We also noticed that at constant aluminum and heat input, high Ni favors martensite (and perhaps bainitic high temperature β transformation products) while high Fe favors the formation of α in various forms. The addition of Cr helps to suppress α, in both the deposit and reheated zone and reduces differences between those two zones. This is shown in Fig. 5. Titanium and zirconium additions produced laser surface melted microstructures which were similar to each other and much different from other structures. Both additions seemed to support the formation of α and a multiphase equiaxed structure (this is shown in Fig. 6.).

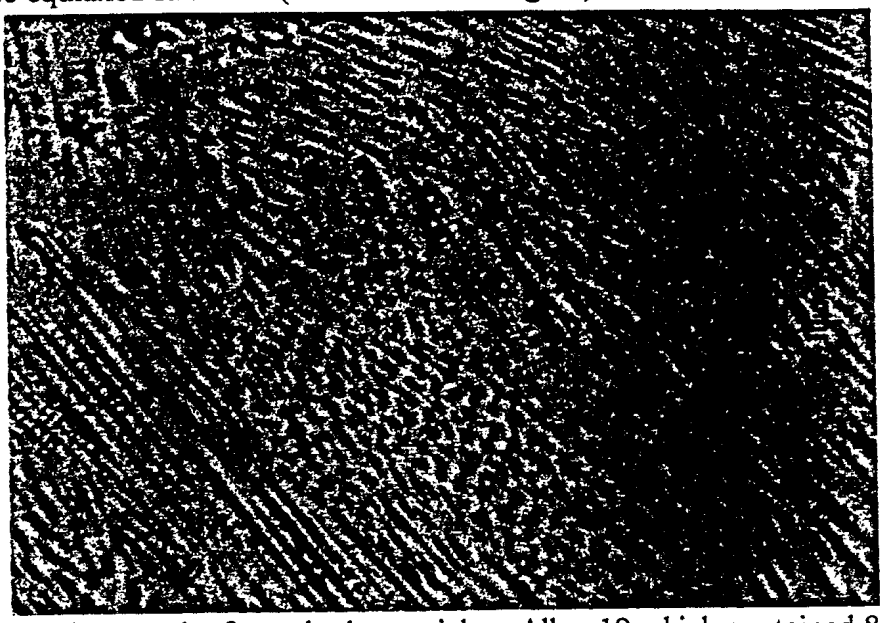

Figure 3. Optical micrograph of remelted material on Alloy 19 which contained 8.8-Al, 4.6-Ni, 6.2-Fe, 1.1-Mn.

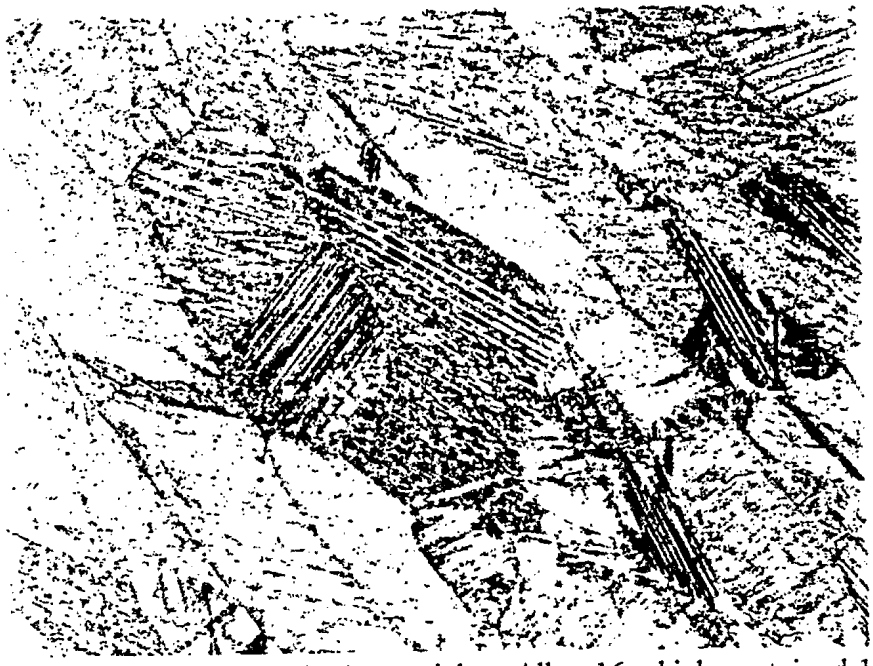

Figure 4. Optical micrograph of remelted material on Alloy 16 which contained 11.3-Al, 4.1-Ni, 5.0-Fe, 1.0 Mn.

Figure 5. Optical micrograph of remelted material on Alloy 21 which contained 9.61-Al, 5.16-Ni, 5.6-Fe, 1.1-Mn, 0.61 Cr.

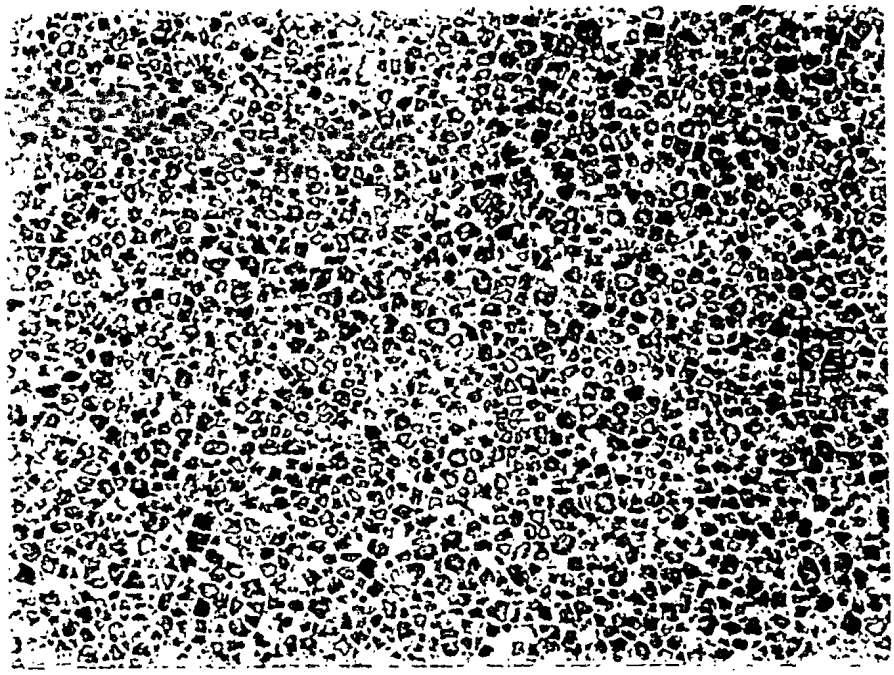

Figure 6. Optical micrograph of remelted material on Alloy 14 which contained 10.0 Al, 5.05 Ni, 6.3 Fe, 0.31 Mn, 1.08 Ti.

Limited electron microscopy on these alloys has been carried out. Examination of Alloy 21, laser surface melted with a heat input of 300 J/mm showed that this alloy contained predominately martensite and bainite with structures similar to those found in a Cu-9.0Al-4.6Ni-3.9Fe-1.2Mn laser cladding deposit produced with a heat input of 150 J/mm [36]. A typical region is shown in Fig 7. This Figure reveals a predominately two-phase microstructure containing martensite plates along with α or bainite. Numerous small (~20 nm) precipitates are also present. In-situ x-ray microanalysis indicated these precipitates are Fe and Cr rich, containing up to 20 % Cr. In contrast, Alloy 27 which contains Ti and Zr as well as Cr additions, exhibits a different microstructure when laser surface melted with the same 300 J/mm heat input. As shown in Fig. 8, the microstructure again consists mainly of α and martensite. However in this alloy, α is present with a more equiaxed morphology and a greater volume fraction. Several additional phases are also observed including small Fe/Cr rich precipitates similar to those found in Alloy 21 as well as somewhat larger Fe/Zr-rich particles. Further TEM studies are in progress to characterize the crystallographic structure of the precipitate phases in these alloys.

3.2. Corrosion Potential Measurements

The results of the corrosion potential measurements are summarized in Table 3. The results for Alloy 4, which was tested in both the as received condition (i.e. with the high temperature oxides still intact) as well as after grinding shows that the corrosion potential of the oxide film from welding is different from that of a ground sample. This supports suggestions in an earlier paper that oxides from welding may play a role in localized corrosion [30]. It is also interesting that the corrosion potential of surfaces produced at a lower heat input of 65 J/mm was generally more negative than those produced at a higher heat input 300 J/mm. This may be a result of a higher volume fraction of more metastable phases or of less tempering of the

metastable phases in the more rapidly cooled lower heat input case. Further investigation of this observation is being carried out. The corrosion potentials of the higher heat input specimens, for all alloys examined, are similar to those of other marine copper alloys.

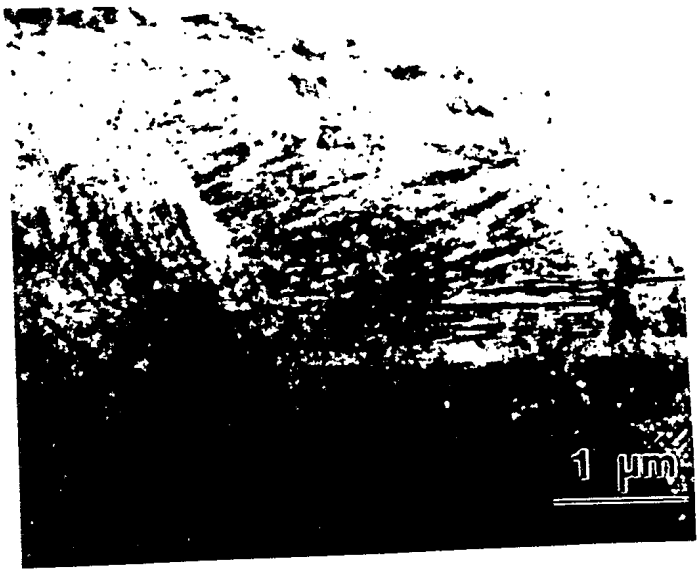

Figure 7. Transmission electron micrograph of remelted material on Alloy 21 revealing a predominately two-phase microstructure of martensite (dark irregular plates) and α (light rod like features). A high density of cuboidal Fe/Cr-rich precipitates is also present.

Figure 8. Transmission electron micrograph of remelted material on Alloy 27 revealing an α plus martensite structure. Compared with the microstructure shown in Fig. 7, there is more α and the α is more equiaxed. A high density of precipitates is also present.

In making the corrosion potential measurements, we noticed that the oxide films from welding in many cases were very hard and electrically resistant. Measurements were made with a hand held electrical resistivity meter. Those listed in table 1 as having high resistance generally could not be penetrated with the pointed steel prods of the hardened steel probes. With a few exceptions, the higher resistivity surface film seems to be favored by higher aluminum and higher heat input as well as by the presence of the experimental alloying additions Ti, Zr or Cr.

Table 3. Corrosion Potentials E_{corr} of Various Experimental Alloys with Laser Treated Surfaces in Deaerated Sea water at 25°C

Alloy Number	Laser Treatment					
	Heat Input = 65 J/mm			Heat Input = 300 J/mm		
	E_{corr} versus SCE [mV]		Surface	Ecorr versus SCE [mV]		Surface
	1st Reading	2nd Reading	Resistance	1st Reading	2nd Reading	Resistance
1	-387	-385	Low	-335	-336	High
2	-381	-381	Low	-336	-335	High
3	-454	-454	Low	-354	-356	High
4	-412	-410	Low	-324	-325	High
4[a]	-394[a]	-	Low	-285[a]	-	-
5	-438	-438	Low	-	-	-
6	-	-	-	-	-	-
7	-	-	-	-	-	-
8	-378	-377	Low	-342	-342	Low
9	-479	-478	Low	-353	-355	Low
10	-425	-425	Low	-332	-332	Low
11	-457	-457	Low	-347	-348	Low
12	-	-	-	-	-	-
13	-	-	-	-	-	-
14	-397	-396	High	-287	-288	High
15	-	-	-	-	-	-
16	-	-	-	-	-	-
17	-	-	-	-	-	-
18	-435	-435	High	-339	-340	High
19	-	-	-	-	-	-
20	-311	-312	Low	-349	-349	High
21	-404	-403	High	-339	-340	High
22	-	-	-	-	-	-
23	-411	-410	High	-319	-319	High
24	-409	-409	High	-299	-300	High
25	-412	-412	High	-340	-340	High
26	-	-	-	-	-	-
27	-415	-415	High	-315	-316	High

3.3. Cavitation Erosion

So far in the evaluation of cavitation erosion behavior we have examined specimen topography and erosion performance. Often in cavitation erosion experiments , a porous surface is produced with fairly general attack. For nickel aluminum bronze this is true of both castings and conventional welds. However in a previous study [3], we noticed laser welds were preferentially eroded at the reheated zones during cavitation erosion. This allowed each laser pass to be seen and as a result the specimen appeared to have a raster pattern on its surface. In the cavitation erosion tests on the experimental alloys, four basic surface morphologies were observed on the specimens. Table 4 lists the morphologies which dominated for each specimen tested. Morphology (c) indicates that the tested surface exhibited a raster pattern with dispersed cracks. These cracks were often faintly visible on the pretest polished specimen surface. Three alloy compositions (6,9,13) exhibited cracking. Table 1 indicates that the aluminum content in these three specimens was over 12 weight percent. The only specimen with more than 12.0 percent Al which did not crack was specimen 15. Of these four specimens, specimen 15 was the only alloy where the percentage of Fe exceeded the percentage Ni. The only alloy composition to exhibit the porous morphology (p) expected on cavitation eroded nickel aluminum bronze was Alloy 19. This alloy had the lowest amount of Al content (8.8 percent) of any studied. It was also the only alloy which had a cellular dendritic microstructure. All the remaining specimens exhibited the raster wear pattern (r) observed in previous studies [6]. The zirconium bearing specimens tended to be much smoother (r/s), though the raster pattern could still be seen.

Table 4 and Figure 9 indicate that the overall erosion performance of an alloy depended strongly on its aluminum content. All alloy compositions containing in excess of 10.7 percent Al performed exceptionally well regardless of the visual appearance of the tested surface of the specimen. The only composition producing equivalent performance with less than 10.7 percent Al was specimen 25 which contained 9.64 percent Al and 1.72 percent Cr. The lowest performing alloys of the compositions listed in Table 1 were either low in Al (less than 9 percent) or contained additions of titanium of greater than 2 percent.

For the alloys tested, it is observed that chemistries which produce above average overall performance (i.e. time to 25 μm penetration) generally have both above average incubation times and above average erosion rates. Several of the alloy compositions have exceptionally low erosion rates (low slope) when compared to the standards recommended in ASTM G-32. The low erosion rates observed tend to reduce the sensitivity of the linear extrapolation method used by ASTM G-32 to determine the incubation time. As well, the surface is not homogenous. Thus, on some specimens the reheated zones and the as deposited material behaved differently. As a result, in simplification the measured curves could be considered a sum of the curves for each weld zone.

We are looking forward to the results of transmission electron microscopy studies on these alloys, because these may help us to understand what role the type and density of planar boundaries and other microstructural features played in determining the topography and cavitation erosion resistance of different weld zones and alloys.

Table 4 - Summary of the cavitation results contained in Appendix B.

Specimen ID	Incub Time (hrs)	Max. Rate (um/hr)	Specimen ID	Incub Time (hrs)	Max. Rate (um/hr)	Avg Incub Time (hrs)	Rank	Avg Rate (um/hr)	Rank	Elapsed Time to 25 um (hrs)	Rank
1A(r/s)	1.01	2.53	1B(r/s)	1.14	2.35	1.075	22	2.44	21	11.3209	21
2A(r)	2.55	1.42	2B(r)	2.56	1.49	2.555	7	1.455	11	19.7371	10
3A(r)	1.77	1.97	3B(r)	1.44	1.97	1.605	17	1.97	19	14.2954	19
4A(r)	2.62	1.59	4B(r)	2.55	1.56	2.585	6	1.575	14	18.458	12
5A(r)	2.00	1.82	5B(r)	1.45	1.76	1.725	13	1.79	16	15.6915	16
6A(c)	3.32	1.21	6B(c)	3.25	1.09	3.285	2	1.15	6	25.0241	4
7A(r)	2.49	1.04	7B(r)	2.30	1.05	2.395	9	1.045	2	26.3184	3
8A(r)	1.83	2.04	8B(r)	1.91	1.79	1.87	12	1.915	17	14.9248	17
9A(c)	3.06	1.07	9B(c)	1.94	1.22	2.5	8	1.145	5	24.3341	6
11A(r)	2.01	1.13	11B(r)	2.06	1.09	2.035	10	1.11	4	24.5575	5
12A(r)	4.45	1.44	12B(r)	4.03	1.27	4.24	1	1.355	8	22.6902	7
13A(c)	2.53	1.01	13B(c)	3.80	1.11	3.165	3	1.06	3	26.7499	2
14A(r/s)	2.02	1.56	14B(r/s)	f/t	f/t	2.02	11	1.56	13	18.0456	14
15A(r)	2.64	0.98	15B(r)	3.09	0.99	2.865	4	0.985	1	28.2457	1
16A(r)	2.78	1.33	16B(r)	2.50	1.48	2.64	5	1.405	9	20.4336	9
17A(r)	1.40	1.93	17B(r)	1.78	1.94	1.59	18	1.935	18	14.5099	18
19A(p)	1.07	5.59	19B(p)	0.93	5.87	1	24	5.73	25	5.363	25
20A(r)	1.71	1.45	20B(r)	1.21	1.37	1.46	19	1.41	10	19.1905	11
21A(r)	1.71	1.46	21B(r)	1.71	1.59	1.71	14	1.525	12	18.1034	13
22A(r)	1.86	1.70	22B(r)	1.48	1.73	1.67	15	1.715	15	16.2473	15
23A(r/s)	1.17	2.70	23B(r/s)	1.20	2.60	1.185	21	2.65	22	10.619	22
25A(r)	1.67	1.31	25B(r)			1.67	16	1.31	7	20.754	8

() letter in brackets refers to specimen surface morphology.
n/t - indicates weight loss numbers were influenced by porosity in specimen.
f/t - indicates a fatigue crack formed in the specimen before enough useful data could be recorded.

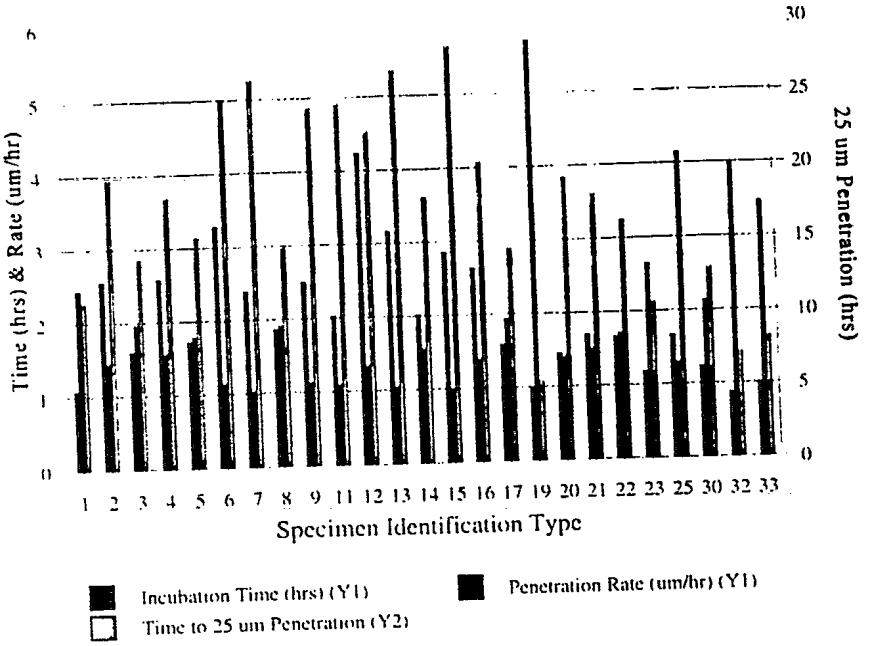

Figure 9. Cavitation erosion behavior

3.4. Temper Resistance

Typical results of the tempering experiments are shown in Figure 10. Briefly, specimen sets with higher contents of aluminum (≥ 11.30%) appear to have the greatest resistance to tempering. These sets also had high manganese contents (≥ 0.95%) and high nickel to iron ratios. In terms of the additions of Cr, Ti, Zr, the results suggest that Cr has little effect and Ti and Zr may have an effect in modifying behavior at long times and a temperature of 600°C. Here a tempering reaction seems to be occurring in the Zr containing alloy long after it is complete in the conventional one. This latter observation could be significant if a standard corrosion inhibiting heat treatment were applied to alloys containing Ti or Zr. These experiments are summarized in more detail elsewhere. Further work on the tempering and phase transformation behavior of these alloys, by metallography, hot stage microscopy, differential thermal analysis and quench dilatometry is planned. Eventually it is hoped that tempering-transformation diagrams will be developed, along with a clearer understanding of the reactions involved in tempering of these alloys.

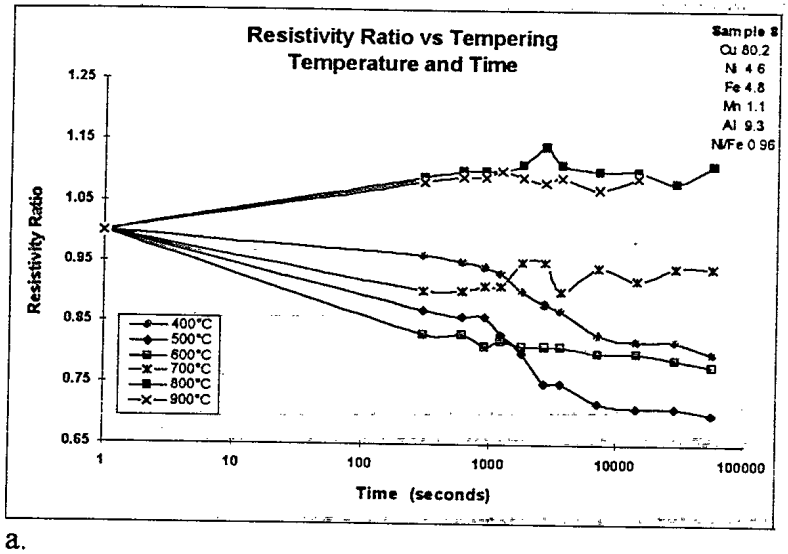

a.

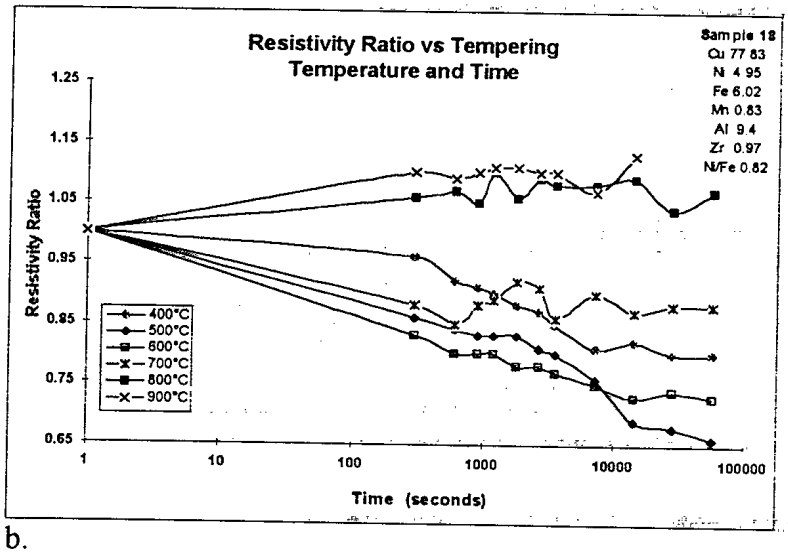

b.

Figure 10. Typical results of resistivity measurements for otherwise similar specimens with (a)and without Zr (b).

4.0 CONCLUSIONS

Work to develop an optimum alloy for low heat input welding of nickel aluminum bronze has been started. Metallography shows that the structure and hardness of the remelted material and the reheated zones are sensitive to Ni/Fe as well as aluminum content. At the lowest aluminum content studied, the as deposited microstructure was cellular dendritic, the hardness was low and the cavitation erosion resistance was the worst measured among the alloy sets. As the aluminum content increased, the tendency of the reheated zone to soften was reduced, the hardness increased and the amount of α in the remelted and reheated zones was reduced. Also as aluminum content increased, the cavitation erosion resistance increased. High nickel

seemed to favor a martensitic and bainitic high temperature transformation products, while high iron seemed to favor the formation of α in the remelted material. The addition of chromium seemed to increase the hardness of both remelted and reheated zones, suppressed the formation of α, and improve cavitation erosion resistance over that in otherwise equivalent alloys without chromium. The role of titanium and zirconium is less clear. Zirconium at least seems to promote the formation of a two phase α plus martensite structure in the remelted material. Cavitation erosion resistance seems to be lower, but it is interesting that the presence of this alloying element promotes a smoother surface during cavitation erosion. Technologically this could be useful from the perspective of the interaction between cavitation erosion and corrosion fatigue.

In summary, earlier work showed that laser welding is a technically viable means of improving and repairing high value components. It also showed that even with conventional consumable compositions, property improvements could be achieved. The work reported here reveals there are several routes by which an optimum alloy for low heat input welding of nickel aluminum bronzes might be developed and that results so far are promising.

5.0 REFERENCES.

1. P.J. Macken and A.A. Smith, *The Aluminum Bronzes, Properties and Production Processes*, CDA Publication 31, Herts, England, 1966.

2. F.L. LaQue, *Marine Corrosion*, Wiley, New York, 1975.

3. *Rules for Building and Classing Steel Vessels*, American Bureau of Shipping, Paramus, New Jersey, 1990, Section 37/2.

4. *Rules and Regulations for the Classification of Shipping*, Lloyds Resister of Shipping, London, England, 1978, Part 5, Chapter 7, Sections 2.1 and 3.1 and Part 2, Chapter 9, Section 1.

5. C.F. Zanis and R.J. Ferrara, *AFS Trans*, 1974, vol. 53, pp. 71-78.

6. J.C. Rowlands,., *Proc. 8th International Congress on Metallic Corrosion*, Mainz, Germany, 1981, pp.1346-1351.

7. R.J. Ferrara and T.E Caton, 1981, *Proc of Corrosion 81*, NACE, Houston, Texas, 1981, Paper 198.

8. E.A. Culpan and G. Rose, *British Corrosion Journal*, 1979, vol. 14, pp. 160-166.

9. C.W. Draper, *Lasers in Metallurgy*, The Metallurgical Society, Warrendale, PA, 1981, pp. 21-31.

10. C.W. Draper, *J. Mat. Sci*, 1981, vol. 16, pp. 2774 to 2780.

11. C.W. Draper, J.M. Vandenberg; C.M. Preece, and C.R. Clayton, *Rapidly Solidified Amorphous and Crystalline Alloys*, 1982, Elsevier, New York, pp. 529-533.

12. C.W. Draper and S. P. Sharma, *Thin Solid Films*, 1981, vol. 84, pp. 333-340.

13. C.W. Draper, S. P.Sharma, J. L. Yeh, and S. L. Bernasek, *Surface and Interface Analysis*, 1980, Vol. 2, pp. 179-182.

14. R.J. Taylor; D.A. Weston, G.M. Wright, and B.W. Turnbull, Sept. 1987, *Corrosion Australasia*, pp. 12-17.

15. N. Dubnyakov, I. B. Malysheva, and S. F. Pulim, *Sov. J. Friction and Wear*, 1986, vol. 7, Translation, New York, Allerton Press, pp. 70-76.

16. F. Hasan, A. Jahanafrooz, G.W. Lorimar, N. and Ridley, *Met. Trans.*, 1982, vol 13A, pp. 1337-1345.

17. Y. Liu, J. Mazumder, and K. Shibata, *Met. Trans.*, 1994, vol. 25A, pp. 37-46.

18. Y. Liu, M.E. Mochel, J. Mazumder and K. Shibita, *Acta Met.*, 1994, vol. 42, pp. 1763-1768.

19. Y. Liu, J. Mazumder, and K. Shibata, *Met.Trans. B*, 1994, vol. 25B, pp. 749-759.

20. C.V. Hyatt, K.H. Magee, J. Hewitt and T. Betancourt, Laser Weld Cladding of Nickel Aluminum Bronzes, in *Abstracts and Summaries of the 2nd CF/CRAD Meeting on Naval Applications of Materials Technology*, 1995, J.R. Matthews, ed., Defence Research Establishment Atlantic, Dartmouth, Nova Scotia, pp. 226-252.

21. C.V. Hyatt, and K.H. Magee, in *Proceedings of Advanced Methods of Joining New Materials II*, The American Welding Society, Miami, Florida, 1994, pp. 111-126.

22. D.E. Bell, Master of Science Thesis, *Microstructural Development and Corrosion Resistance of Laser-Welded Nickel Aluminum Bronze*, Pennsylvania State University, 1993.

23. K. Petrolonis, *Laser Welding and Continuous Cooling Studies of Nickel Aluminum Bronze*, Master of Science Thesis, The Pennsylvania State University, 1993.

24. P.J. Oakley and N. Bailey, in *Proc. International Conference on Power Beam Technology*, 1986, The Welding Institute, Cambridge, England, pp. 301-314.

25. F. Hansan, G.W. Lorimar and N. Ridley in *Proceedings Conference on Phase Transformations*, 1987, Cambridge, U.K., pp. 131-134.

26. D.E. Bell, K. Petrolonis and P.R. Howell, in *Proc. International Trends in Welding Science and Technology*, S.A. David and J.M. Vitek Eds, Gatlinburg, TN, pp. 301-305.

27. D.E. Bell, T.A. Marsico, K. Petrolonis, P. E. Denney and P.R. Howell, *Metallography: past, Present and Future*, ASTM STP 1165, 1995, G.F. Vander Voort, F.J. Warmoth, S.M. Purdy and A. Szirmae, Eds., ASTM, Philadelpia, Penn., pp. 327-434.

28. J. Hewitt, Laser Weld Overlaying of Marine Components and Alloys, DREA CR/95/525, Defence Research Establishment Atlantic, Dartmouth, Nova Scotia.

29. J. Hewitt, V.E. Merchant, C. Hyatt, and D.O. Morehouse, Laser Beam Welding of Nickel Aluminum Bronze with a Fine Wire Feeder, Presented at the 78th Annual AWS Convention, Written Version of the Paper is being prepared for the Welding Journal.

30. C.V. Hyatt, K.H. Magee, and T. Betancourt, The Effect of Heat Input on the Microstructure and Properties of Nickel Aluminum Bronze Laser Clad with a Consumable of Composition Cu-9.0Al-4.6Ni-3.9Fe-1.2Mn, In internal review, for submission to Metallurgical Transactions.

31. K.H. Magee, "Laser Cladding of Marine Copper Alloys," DREA CR/94/424, Defence Research Establishment Atlantic, Dartmouth, Nova Scotia 1994..

32. P. Brezina, *International Metals Reviews*, 1982, vol. 27, pp. 77-120.

33. S. Kumar, International Metals Reviews, 1990, 35, 6, 294-327.

34. C.V Hyatt, *Review of Literature Related to Microstructural Development During Laser Surface Engineering of Nickel Aluminum Bronze, DREA Technical Memorandum*, TM/96/227, 1996, Defence Research Establishment Atlantic, Dartmouth, Nova Scotia.

35. J.C. Bennett, Microstructural Characterisation of Laser-Clad Nickel Aluminium Bronze Alloys by Transmission Electron Microscopy, DREA/CR/96/442, Defence Research Establishment Atlantic, Dartmouth, Nova Scotia, 1996.

36. J.C. Bennett and C.V. Hyatt, *TEM Study of NiAl Bronze Laser-Weld Claddings*, Proceedings of the 1997 Microscopical Society of Canada General Meeting, 1997, vol. 24. pp70-71.

37. *ASTM Standard G5-87, Standard Reference Test Method for Making Potentiostatic and Potentiodynamic Anodic Polarization Measurements*. 1987 Annual Book of ASTM Standards, Vol. 03.02. pp. 124-131, Philadelphia, PA.

38. *ASTM Standard G32-85, Standard Method of Vibratory Cavitation Erosion Test. 1987 Annual Book of ASTM Standards*, Vol. 03.02, pp. 187-194. ASTM, Philadelphia, PA.

39. C.V. Hyatt and B. Armstrong, Metallographic Characterization and Microhardness Testing on Experimental Alloys Laser Surface Melted With Heat Inputs of 10, 65 and 300 J/mm. DREA Lab Note, In Prepartion.

40. G. Pelletier, C.V. Hyatt, "Tempering Resistance of Experimental Nickel Aluminum Bronze Alloys", DREA DL/RN/97/6.